



# Determining constitutive behavior of the brain tissue using digital image correlation and finite element modeling

Amir Mohammad Felfelian<sup>1</sup> · Amirhosein Baradaran Najar<sup>1</sup> · Reza Jafari Nedoushan<sup>1</sup> · Hossein Salehi<sup>2</sup>

Received: 2 February 2019 / Accepted: 5 June 2019  
© Springer-Verlag GmbH Germany, part of Springer Nature 2019

## Abstract

Detailed knowledge about the mechanical properties of brain can improve numerical modeling of the brain under various loading conditions. The success of this modeling depends on constitutive model and reliable extraction of its material constants. The isotropy of the brain tissue is a key factor which affects the form of constitutive models. In this study, compression tests were performed on different parts of the sheep brain tissue. Also, the digital image correlation (DIC) method was utilized to investigate the direction dependency of brain parts considering their microstructures. To this aim, the DIC method was employed to measure the transverse strain of two lateral sides of the tissue samples. The results of DIC method revealed that the brain stem and corona radiata were isotropic, while the mixed white and gray matter showed an unrepeatable behavior depending on the extracted sample. To examine and validate DIC method, stress–strain diagrams were also used to investigate the isotropy. It could be concluded that axonal fibers had no reinforcing role in the brain tissue. Furthermore, the DIC method indicated incompressibility of the brain tissue. Then, the significance of using a correct method to extract the material constants of brain was discussed. In other words, the effect of the real boundary conditions in experiments, which was neglected in most previous studies, was taken into account here. Finally, the particle swarm optimization algorithm along with the finite element modeling was used to estimate the hyper-viscoelastic constants of different parts of the brain tissue.

**Keywords** Brain tissue · Mechanical characterization · Reinforcing role of axons · Digital image correlation · Finite element modeling · Particle swarm optimization

## 1 Introduction

Brain injuries, which can be caused by anything from an infection to a car accident, are known as irreparable damages. Mechanical modeling can be employed as a powerful predictive instrument for such damages (Goriely et al. 2015). Biomechanical modeling offers great contributions to scientific research including: the prediction of the exact location and intensity of induced damage (Wright et al. 2013), development of criteria for tissue damage (Cloots et al. 2012), and improvement in protective equipment (Wu et al. 2016). Biomechanical modeling of brain tissue is mostly affected by its constitutive behavior (Cloots et al. 2013). In other words,

when using mechanical modeling, the precision of the constitutive model including both the constitutive relations and the material constants, would directly influence the results.

To investigate the brain constitutive behavior, extensive experimental studies have been conducted on various brain tissues including human (Budday et al. 2017a; Jin et al. 2013; Shuck and Advani 1972; Chatelin et al. 2012; Fallenstein et al. 1969; Estes and McElhaney 1970; Galford and McElhaney 1970; Donnelly and Medige 1997; Franceschini et al. 2006), porcine (Velardi et al. 2006; Thibault and Margulies 1998; Prange and Margulies 2002; Miller and Chinzei 1997, 2002; Miller 1999; Rashid et al. 2012, 2013, 2014; Van Dommelen et al. 2010), bovine (Budday et al. 2015; Darvish and Crandall 2001; Bilston et al. 2001), sheep (Anderson et al. 2003; Lewis et al. 1996; Pamiljans et al. 1962), and rat (Karimi and Navidbakhsh 2014; Karimi et al. 2014; Elkin et al. 2010; Finan et al. 2012; Christ et al. 2010) brain. Since performing mechanical experiments on brain tissue is associated with several uncertainties and complexities (Budday et al. 2017a), there is little consensus on

✉ Reza Jafari Nedoushan  
rjafari@cc.iut.ac.ir

<sup>1</sup> Department of Mechanical Engineering, Isfahan University of Technology, Isfahan 84156-83111, Iran

<sup>2</sup> Department of Anatomical Sciences, School of Medicine, Isfahan University of Medical Sciences, Isfahan, Iran

estimation of the properties of the brain tissue. Findings of the previous research reveal the disparity of conclusions on the effect of loading direction and location of the sample in the brain, though researchers have reported similar stiffness values (Budday et al. 2017a). Meanwhile, the reinforcing role of axon fibers in the brain tissue has not been thoroughly investigated yet. In a vast majority of studies with a micromechanical view, the tissue has been considered as an anisotropic material (Jin et al. 2013; Velardi et al. 2006; Chatelin et al. 2011; Arbogast and Margulies 1999; Wright et al. 2013; Cloots et al. 2011; Feng et al. 2017; Giordano et al. 2014; Giordano and Kleiven 2014; Cloots et al. 2013; Garcia-Gonzalez et al. 2018; Aumedieu et al. 2001; Ning et al. 2006; Hrapko et al. 2008). In contrast, in some other studies, it was proven that the presence of axon fibers has no effect on the mechanical properties of the brain tissue (Budday et al. 2017a, b; Miller and Chinzei 1997; Miller 1999; Pamiljans et al. 1962; Karimi and Navidbakhsh 2014; Miller et al. 2000; Mihai et al. 2015; Javid et al. 2014; Tse et al. 2014). Some of them employed diffusion tensor imaging (DTI) to determine the orientation of axon fibers in the examined brain samples (Budday et al. 2017a; Chatelin et al. 2011; Arbogast and Margulies 1999; Wright et al. 2013). Determining the reinforcing role of axons may completely change the constitutive model used in computational modeling of the brain.

In addition to the type of the relationships used in constitutive models, another important issue is the correct estimation of the material constants. A vast majority of research on brain tissue has estimated the coefficients of the constitutive models by fitting an analytical relation to experimental data (Budday et al. 2017a; Velardi et al. 2006; Miller and Chinzei 1997). In these studies, a one-dimensional analytical relation was directly fitted on the experimental curve. Only in a few investigations, an indirect method was employed which used a finite element (FE) model to estimate the unknown coefficients (Karimi et al. 2014; Javid et al. 2014).

In the current research, the DIC method was utilized for the first time to investigate the reinforcing role of axon fibers on the mechanical behavior of brain tissue. While two different samples are required to examine the anisotropic behavior of the tissue via stress–strain diagrams, the DIC method can examine it through experimentation on a single specimen. As the brain tissue is the most complex organ, changing the laboratory samples can intensely affect the results, and this fact can be an explanation to divergent findings of the previous studies.

More than 100 tests were conducted on the different parts of the brain sample to determine the anisotropic behavior of brain tissue and extract its material constants. All the experiments were conducted on the fresh sheep brain tissues to prevent the adverse effects of preservative solutions. After determining the anisotropic property of the brain tissue, its

mechanical properties were extracted. To this aim, firstly the inefficiency of the direct fitting method was examined. Then, a new approach based on the particle swarm optimization (PSO) algorithm was proposed to estimate the brain tissue properties. Finally, using the finite element (FE) modeling in conjunction with the PSO algorithm, the coefficients of the constitutive model were estimated and reported for different parts of the brain tissue at different rates.

## 2 Materials and methods

### 2.1 Specimen preparation

A total of 30 sheep brains were extracted from adult animals (age between 1 and 2 years). Prior to the experiment, the protocol was confirmed to be in accordance with the Guideline of Animal Ethics Committee of Isfahan University of Medical Sciences.

Experiments were completed within 3–4 h to minimize the postmortem time. The extracted brains were kept in the phosphate buffer saline (PBS) at a temperature of 3–7 °C so as to preserve the freshness of the tissue. All laboratory instruments were wetted in the same solution to prevent tissue damage or tearing when contacting the tools. Cubic specimens with the length of 5 mm were prepared from the brain samples. Nevertheless, due to the deformable and soft nature of brain tissues, the final dimensions of cubic specimens were recorded prior to compression tests. Further, the axon orientation of different parts of brain was assessed by a general diffusion tensor atlas (Lee et al. 2015).

The design of experiments was based on the axon orientation of the brain parts. Anatomical studies and DTI data indicated that axonal fibers of the brain stem are mostly unidirectional (Fig. 1a). Assuming reinforcing role of axons, this type of orientation can be considered as a transversely isotropic material. Unlike the brain stem, the corona radiata contains multi-directional axons (Fig. 1b). In this study, the dominant fiber direction based on anatomy was into account in the cubic specimens for the corona radiata. For the mixed gray and white matter specimens, there was no specific direction. Table 1 presents the location of the prepared specimens, direction of the loading, and test method.

### 2.2 Experimental setup

The Zwick 1445 tensile test machine was used to perform compression tests. The installed load cell allowed measurement of axial force within the range of 0.01–5 N, with an error of less than 0.02% of the maximum load. During the experimental tests, high quality pictures were taken simultaneously from two views from specimens using two high-speed digital cameras (CANON Eos 80D). The recorded

**Fig. 1** **a** Sample of brain stem, **b** direction of axons in corona radiata

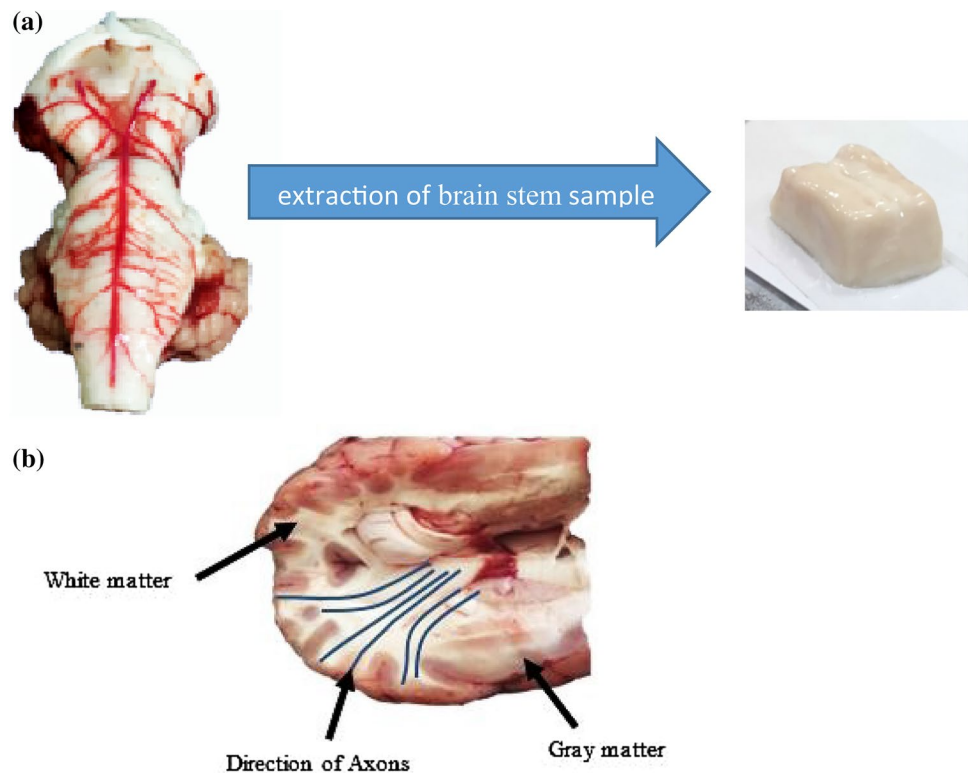


**Table 1** Experimental tests details

Brain part	Number of samples	Displacement direction	Test
Brain stem	10	Along the fiber direction	DIC
Brain stem	10	Perpendicular to the fiber direction	DIC
Brain stem	10	Along the fiber direction	Stress–strain diagram
Brain stem	10	Perpendicular to the fiber direction	Stress–strain diagram
Corona radiata	10	Perpendicular to the dominant fiber direction	DIC
Corona radiata	10	Along the direction of dominant fiber	DIC
Corona radiata	10	Perpendicular to the dominant fiber direction	Stress–strain diagram
Corona radiata	10	Along the direction of dominant fiber	Stress–strain diagram
Mixed white and gray matter	10	–	DIC
Mixed white and gray matter	10	–	Stress–strain diagram

pictures were used to perform DIC analysis. The tests were conducted by specified displacement, with load–displacement plots automatically produced. Before loading the samples, a piece of sand paper was attached to each jaw of the testing device to avoid sample slippage (Fig. 2). In addition, cyanoacrylate bio adhesive (EPIGLUE) was used to stick the sample to the sand paper (Hrapko et al. 2008). Using adhesive could limit the lateral strain of the specimens and reduce the accuracy of the DIC method but due to the sticky property of the brain tissue without adhesion the relative displacement of the specimen and jaw are not definite and can cause difference between samples.

Tests were conducted at room temperature. Firstly, the samples were glued to the lower jaw. Then, the upper jaw moved down slowly until detecting the preload of 10 mN. Thereafter, the upper jaw moved up until the zero preloading. Four cycles per specimen were applied where two cycles functioned as pre-conditioning and the third cycle was used for further data analysis (Budday et al. 2017a). Furthermore, the compression tests were performed with two strain rates (1/60 s and 1/6 s) on each specimen. Note that the DIC method worked properly in the chosen strain rates. Also, these rates lied within the range of loading rates of neurosurgical operations.

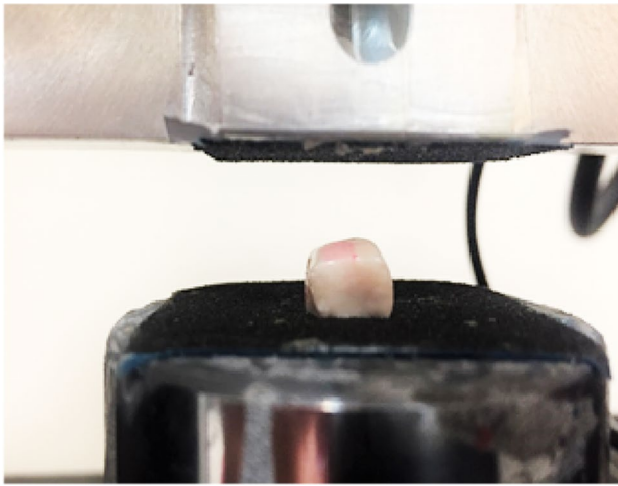


**Fig. 2** Sample placement on the jaw of the tensile test machine

### 2.3 Using DIC method to examine the anisotropic properties of different parts of the brain tissue

Digital image correlation is an optical, noninvasive method to determine the displacements and strains of a deformed sample (Pan et al. 2009). This method tracks the pixels on the surface to compute the displacement vector of surface points and to create all the components of strain tensor in each point.

Numerous applications of DIC have been reported in the literature in particular for biochemical data including determining the Young's modulus and Poisson's ratio of bovine arterial tissue (Zhang and Arola 2004), measuring the full local strain field on porcine and human liver capsules undergoing uniaxial quasi-static tensile tests (Brunon et al. 2010), calculating mechanical properties of human forehead skin subjected to dynamic tensile tests (Annaidh et al. 2012), measuring the acceleration-induced strain fields in porcine brain (Lauret et al. 2009), and investigating brain tissue incompressibility (Libertiaux et al. 2011).

In this part of the research the DIC method is used to investigate anisotropic behavior of the material by measuring the transverse strains in two different sides of the specimens.

#### 2.3.1 DIC setup and procedure

The DIC setup consisted of two cameras mounted on a tripod. The digital DSLR cameras (CANON 80D) with a maximum resolution of  $4000 \times 6000$  and shutter speed of 30-1/8000 s were used to capture photographs. The arrangement of cameras with respect to the sample is displayed in Fig. 3 Further, an appropriate lighting level on samples was provided using three LED lamps. The Zwick 1445 tensile test machine was used to apply displacement on the tissue.

Surface preparation of the specimens was required before performing DIC method. Thus, a speckle pattern was applied through a three-step procedure (Libertiaux et al. 2011). At first, a white background was sprayed on the sample surfaces. Then, to prevent light reflections, which results in local loss of data points, talcum powder was shuffled on the white background. Finally, random black spots were made through spraying procedure. Figure 4a illustrates the suitable pattern provided on a sample. Attempt was made to create patterns on the samples with high density and regular distribution of spots (Libertiaux et al. 2011; Zhang and Arola 2004).

In DIC method, a network of points was placed on a facet in neighborhood of each material point (Fig. 4b). Then, a correlation algorithm was employed to identify the position of each point in the two images and to measure the points' displacements with the accuracy of one percent of a pixel. Finally, the strain components, velocity, and acceleration could be calculated from displacements. Once the images of samples were captured, the required analysis was done on the laboratory samples using the commercially available imaging software package GOM Correlate (Ver. 16). The GOM Correlate software is especially useful for digital image correlation.

#### 2.3.2 Investigating the anisotropic behavior of the brain parts using DIC method

To investigate the anisotropic behavior of the brain stem using DIC method, the compression tests were performed in the direction of axonal fibers and perpendicular to them. Then, the strains were measured and compared at two lateral sides. Figure 5 reveals the possible orientation of the axonal fibers in specimens of the brain stem, related to the loading direction. In this figure, the Y-axis is considered as the loading direction. In the case of applying load along the axonal fiber direction, normal vectors of faces 1 and 2 were perpendicular to the axon fibers (Fig. 5a). When applying load perpendicular to the fiber direction, axonal fibers were oriented perpendicular to the face 2, while they were oriented parallel to the face 1 (Fig. 5b). Assuming the reinforcing role of the axons, in the former case one can expect similar strain values measured from both lateral sides, while in the latter case the lateral strain values will be different. These two types of sample orientation and strain measurements would determine the reinforcing role of the axonal fibers. However, axonal orientation of corona radiata is not unidirectional. Accordingly, a protocol like brain stem was followed to investigate the direction dependency of the corona radiata using DIC method.

As a vast majority of the related literature has assumed the gray matter as isotropic (Budday et al. 2017a; Velardi et al. 2006; Miller and Chinzei 1997; Miller 1999; Miller

**Fig. 3** Experimental setup to record compression of sheep brain sample; **a** front view, **b** upper view

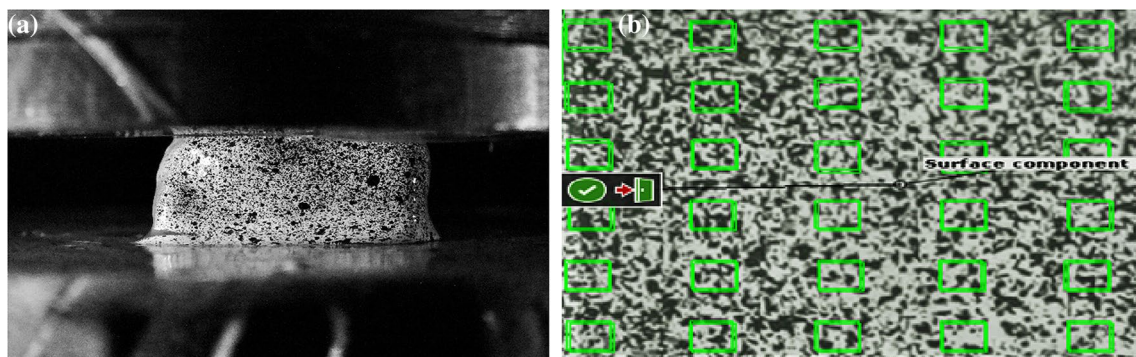
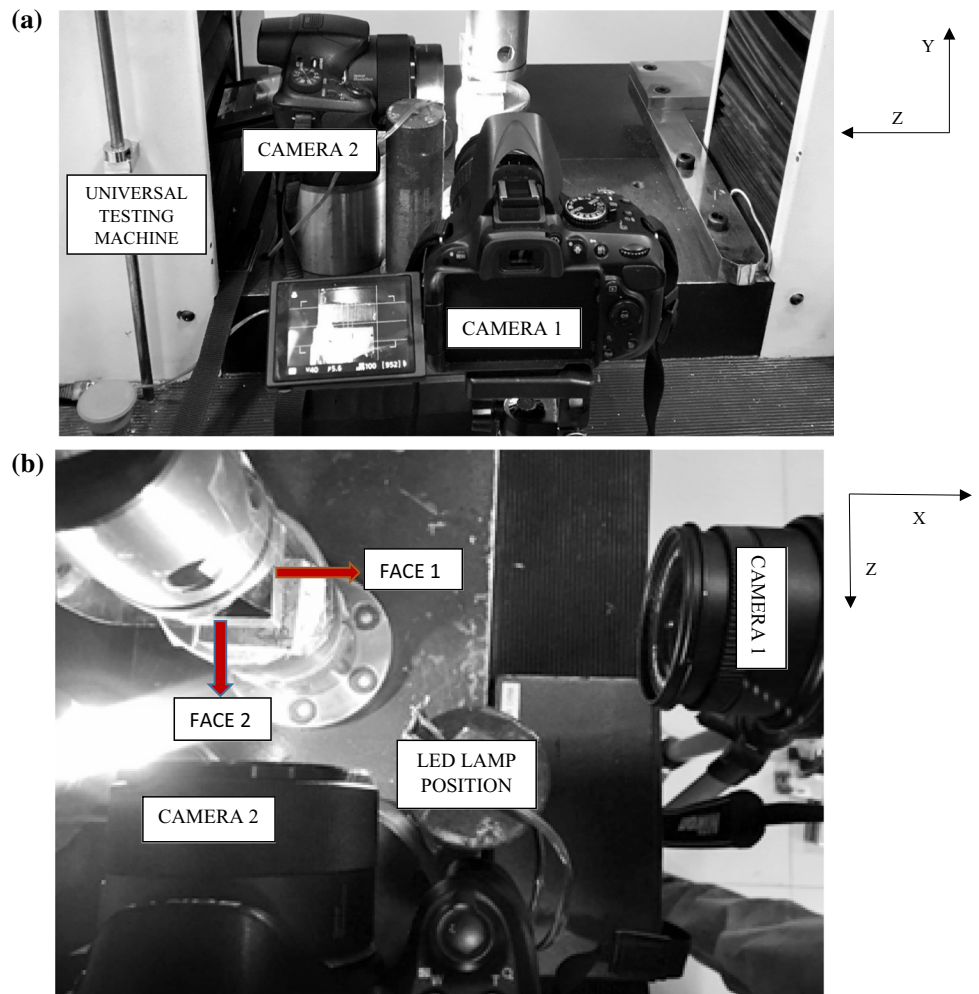


**Fig. 4** DIC implementation; **a** suitable pattern on a sample under compression, **b** network of points on a sample in GOM correlate software

and Chinzei 2002; Karimi et al. 2014), in the present research the same assumption was made. Thus, we began to investigate the isotropic behavior of mixed white and gray matter. In some studies, due to the small size of the brain parts, a mixture of these two matters was examined and the results were reported as the behavior of the brain

tissue (Miller and Chinzei 1997; Miller 1999; Miller and Chinzei 2002; Karimi et al. 2014). Note that to make a more precise comparison of strains on the two faces of all test samples, the strain on the midline of the faces was measured and compared (Fig. 6). Since the lateral strain of the specimens were limited by top and bottom adhesive,

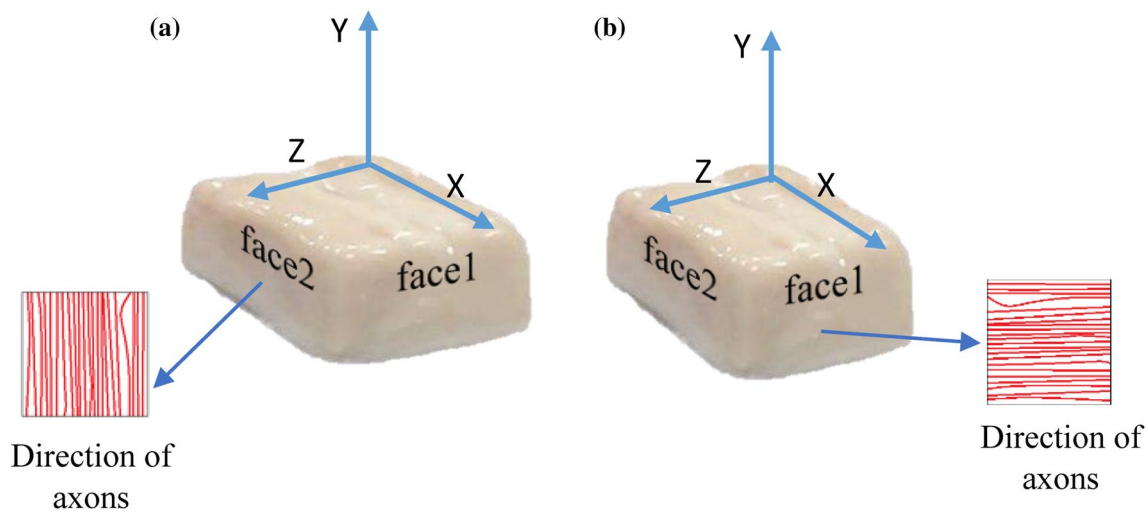


**Fig. 5** **a** Direction of axons in *Y* direction, **b** direction of axons in *Z* direction

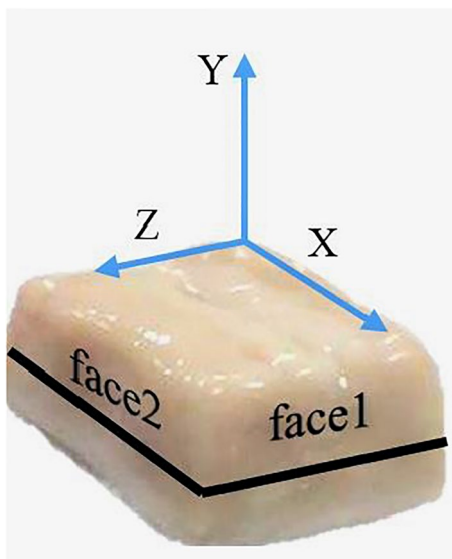


**Fig. 6** Lines where strain analysis was conducted along them

these lines which are far from the adhesive affected region were chosen.

#### 2.4 Investigating the anisotropic behavior of the brain parts using stress–strain diagrams

Another approach to analyze the anisotropic behavior of the brain tissue is to compare the stress–strain curves. Stress–strain curves can be obtained and compared through applying compression loading on samples from two different directions. The strain of 15% (reduction of sample height), at the two strain rates of 1/60 s and 1/6 s, was applied on the sample presented in Table 1. To examine the anisotropic

behavior, the compression loading was applied to 10 specimens of each brain part (brain stem and corona radiata) along the axons' direction (Fig. 5a). However, for the other 10 specimens, the load was applied perpendicular to the axons' direction (Fig. 5b). For the corona radiata specimens, the dominant direction of the axons was considered as the main axonal direction. Attempts were made to extract specimens used in two different loading directions from the same place of the brain parts.

For the mixed white and gray matter, as there is no specific direction and each extracted specimen has a different percentage of white and gray matter, a different protocol was used. In this protocol, tests were conducted on two different sides of one specimen. To control the slipping, rough sand papers without adhesive were used and the process was recorded thoroughly by high-speed/high-resolution cameras.

#### 2.5 Brain mechanical characterization

The approach used to extract the material constants from test results is an important factor which affects the accuracy and effectiveness of these constants. So far, the majority of researchers have employed an analytic function for fitting theoretical relations to experimental data (Budday et al. 2017a; Velardi et al. 2006; Miller and Chinzei 1997). In this method, sample deformation was assumed as totally homogeneous, i.e., the stress/strain values are equal across the entire sample. Therefore, it was only necessary to fit the target analytical diagram in the uniaxial stress mode on the experimental diagram. Although this method is fast and manageable, it does not take into account the effect of the boundary conditions of the test samples. Neither does it consider the existing heterogeneity of the deformation and stress field nor the existed multi-axial stress in the material. As

such, the mechanical data extracted through this method can have a considerable error. In this part of the research, it will be shown that if the material constants extracted through analytical curve fitting method are used in FE modeling of the brain tissue with real boundary conditions, the result will be erroneous. To overcome this shortcoming, FE modeling along with the PSO algorithm will be used to estimate the material constants of the brain tissue from the experimental curves.

### 2.5.1 Constitutive model

In this research, isotropic hyper-viscoelastic constitutive behavior was assumed to model the mechanical behavior of the brain tissue. Ogden hyperelastic model is among the most commonly used models by researchers in investigating the mechanical behavior of body tissues (Budday et al. 2017a; Velardi et al. 2006; Karimi et al. 2014; Mihai et al. 2017). Also, among all hyperelastic isotropic models, only this model is capable of performing analytical curve fitting simultaneously for different modes of loading (Budday et al. 2017a).

The following strain energy relationship was suggested by Ogden (1972):

$$W = \frac{2\mu}{\alpha^2} (\lambda_1^\alpha + \lambda_2^\alpha + \lambda_3^\alpha - 3) \quad (1)$$

From Ogden strain energy relation, nominal stress can be obtained as follows (Velardi et al. 2006):

$$\mathbf{S} = \sum_{i=1}^3 \left( \frac{\partial W}{\partial \lambda_i} - p \lambda_i^{-1} \right) \mathbf{v}^i \otimes \mathbf{u}^i \quad (2)$$

$$p = \frac{2 * \mu * \lambda^{-\frac{\alpha}{2}}}{\alpha} \quad (3)$$

In Eqs. (1), (2), and (3),  $\lambda_1$ ,  $\lambda_2$ , and  $\lambda_3$  are the main stretches;  $\mu$  represents the shear modulus in the infinitely small strain;  $\alpha$  denotes the material constant, and  $\mathbf{u}^i$ ,  $\mathbf{v}^i$  are the eigenvectors of the right and left stretch tensors, respectively. It was also assumed that deformation was homogenous all over the sample. In uniaxial loading, the displacement value was measured to obtain the stretch. If the displacement  $\Delta Y$  at the direction of axis  $y$  is applied to the tissue with the initial length of  $H$ , the stretch along this axis can be calculated by  $\lambda = 1 \pm \Delta Y/H$ . Considering the isotropic behavior and incompressibility of the brain tissue, which will be discussed in the “Results and Discussion” section, it can be shown that  $\lambda_1 = \lambda_2 = \frac{1}{\sqrt{\lambda}}$ . Consequently, the deformation gradient tensor can be obtained as follows:

$$F = \begin{bmatrix} \frac{1}{\sqrt{\lambda}} & 0 & 0 \\ 0 & \frac{1}{\sqrt{\lambda}} & 0 \\ 0 & 0 & \lambda \end{bmatrix} \quad (4)$$

In the uniaxial mode, there is stress only along the loading direction. Therefore, Eq. (2) is simplified to Eq. (5). This equation is the same as the one that is commonly used by researchers analytically for curve fitting of experimental data (Budday et al. 2017a; Karimi et al. 2014).

$$S = \frac{2\mu}{\alpha * \lambda} (\lambda^\alpha - \lambda^{-\alpha/2}) \quad (5)$$

The viscoelastic behaviors of materials are often stated in the Prony series (Eqs. (6) and (7)).

$$G(t) = G_0 \left( 1 - \sum_{i=1}^n g_i \left( 1 - e^{-\frac{t}{\tau_i}} \right) \right) \quad (6)$$

$$k(t) = k_0 \left( 1 - \sum_{i=1}^n k_i \left( 1 - e^{-\frac{t}{\tau_i}} \right) \right) \quad (7)$$

$G_0$  and  $k_0$  represent the shear modulus and bulk modulus, respectively, at  $t = 0$ . Also,  $g_i$ ,  $k_i$ , and  $\tau_i$  are time dependency coefficients. In this research, Prony series with two terms was employed to state the viscoelastic behavior of the material. Accordingly, there were eight unknown coefficients, six of which were attributed to the viscoelastic properties, while the remaining were related to the hyperelastic properties of the material. As the material was incompressible, the number of unknown coefficients was reduced to 6 constants.

### 2.5.2 The finite element modeling of the brain tissue considering the real boundary condition

In this research, “real boundary conditions” suggested that the sticky state of the specimens to the testing setup was considered in the proposed FE modeling. That is, the lower surfaces of the simulated specimen were fixed along axes  $x$ ,  $y$ , and  $z$  (Fig. 7). Similarly, the upper surface of the object was fixed along axes  $x$  and  $z$ , and 15% reduction of the sample height was applied along axis  $y$ .

The current part of present research investigates the effect of ignoring experimental boundary conditions on calculated material constants through the analytical curve fitting method.

Firstly, to show the inefficiency of analytical curve fitting method, Eq. (5) is fitted to the experimental stress–strain diagrams obtained at the strain rate of 1/60 s to calculate the hyperelastic coefficients of the material. Next, the resulting

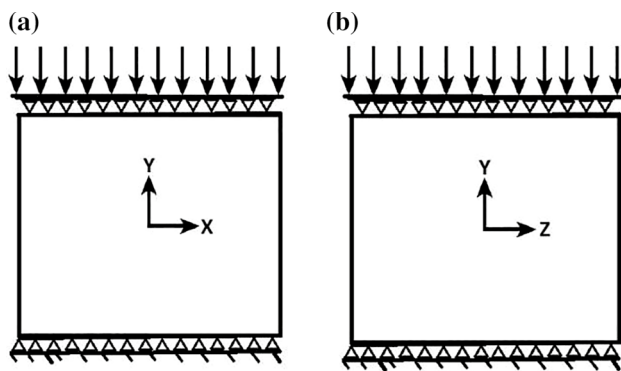


**Fig. 7** Experimental boundary conditions; **a** front view, **b** left view

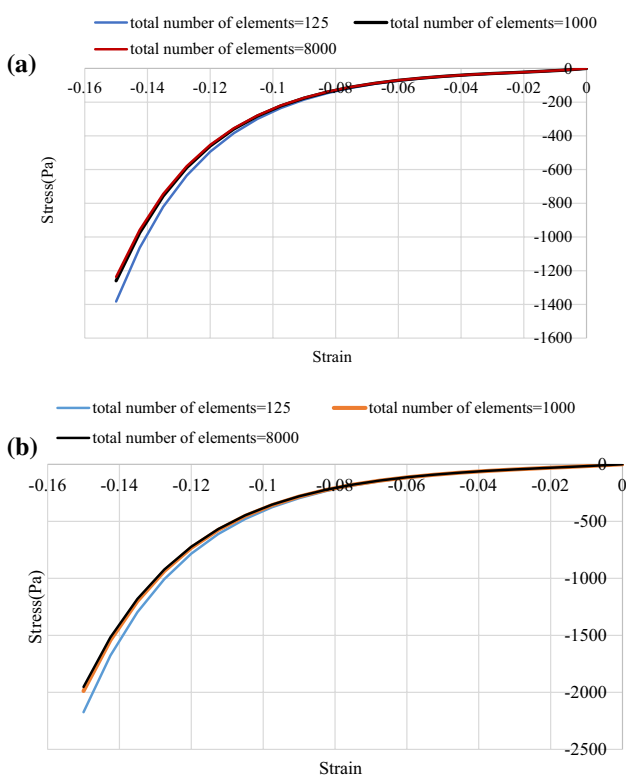


**Fig. 8** Comparison of the simulation results of different mesh sizes for the brain stem at the strain rates of **a** 1/60 s and **b** 1/6 s

hyperelastic constants were used in a FE modeling considering the real boundary conditions. Finally, the experimental results were compared to the simulation results.

To simulate the compression test of brain tissue, a cube with the same dimensions as the test sample was created and the real boundary conditions were applied, as shown in Fig. 7. ABAQUS standard solver was used and 8000 C3D20H elements were used to mesh the part. To investigate the mesh dependency of the model, various mesh sizes were generated and their force versus displacement curves

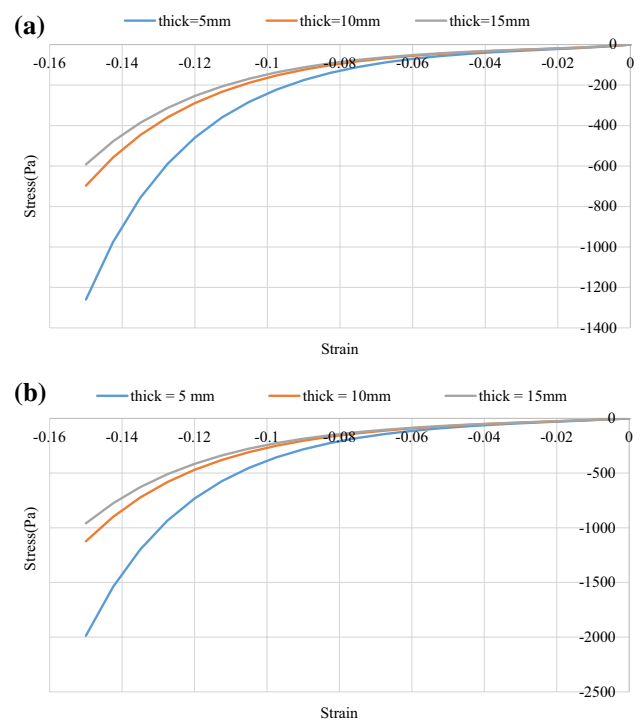


**Fig. 9** Effect of the size of the simulated model on the results of applying pressure on the sample brain stem at the strain rates of **a** 1/60 s and **b** 1/6 s

is compared in Fig. 8. Figure 9 demonstrates that the model dimensions strongly affect the stress–strain curves. Thus, the size of the simulated model should be equal to the test sample size. The results of dependency on the model dimensions indicate the effect of boundary conditions on the distribution of stress and strain of the model.

### 2.5.3 Characterization of mechanical properties of the brain tissue using the PSO algorithm

In this section, the ABAQUS software is used along with Python scripting to properly extract the mechanical constants of the brain tissue from the experimental data. Optimization algorithms can be used to find the best set of material constants in fitting the experimental data. In the present research, the PSO algorithm, which was developed according to the group behavior of particles or birds, was employed. To fit the data through simulation and Python scripting, initially an appropriate target function should be defined. In this study, the target function represented the difference between experimental stress and that of the simulation for various strains.

In the present optimization, the main variables were the hyper-viscoelastic constants of the material. The number of particles and the number of iterations were the input parameters of PSO algorithm. Furthermore, to achieve the



desirable fitness, the numbers of particles and iterations were considered as 25 and 20, respectively. At the end of the solution, the target function which is indeed the error function was reported. Evidently, by increasing the number of particle and iterations, a lower value of the error function or better fitness can be achieved. Equation (8) represents the target function, and Fig. 10 indicates the PSO algorithm flowchart to estimate the mechanical properties of the brain tissue.

$$\text{Error} = \sum_{i=1}^n (S_{\text{simulation}} - S_{\text{experimental}})_i^2 \quad (8)$$

In Eq. (8),  $i$  represents the experimental and simulated stresses for various strains.

### 3 Results and discussion

#### 3.1 Investigating the isotropy of the brain stem, corona radiata, as well as mixed white and gray matter

At first, the results from the examining the isotropy of the brain stem through DIC method will be presented. As previously mentioned in Sect. 2.3, if strain of 15% (reduction of sample height) is applied parallel and perpendicular to axons, then the lateral strain can be measured. Figure 11a shows comparison of strains measured on faces 1 and 2 when loading was applied along the axons' direction. Similarly, Fig. 11b indicates the results of applying load perpendicular

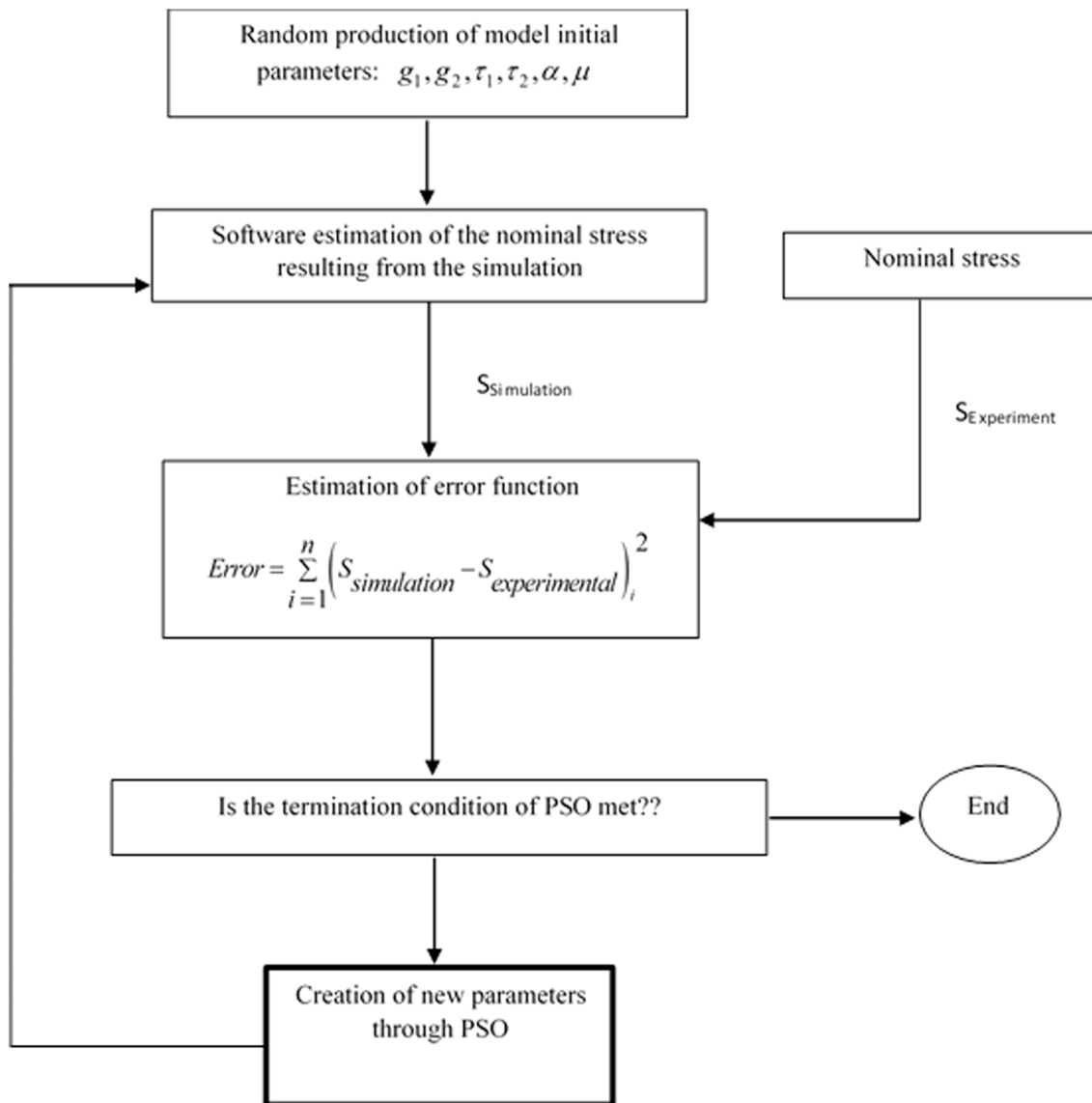
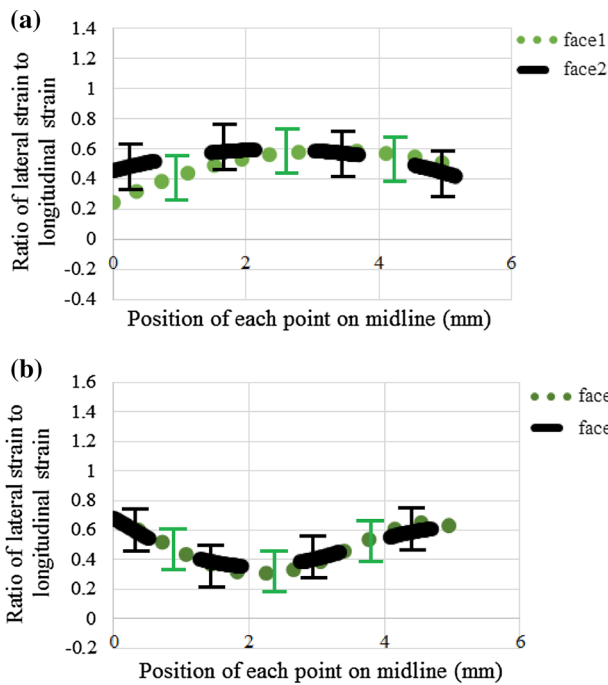


Fig. 10 Determination of the mechanical properties of the brain tissue through a combination of PSO algorithm and ABAQUS software



**Fig. 11** Comparison of the strain measured on face 1 and face 2 for 20 samples of the brain stem through a midline; **a** applied load was parallel to the axons; **b** applied load was perpendicular to the axons

to the axons and the measured lateral strains at the two lateral faces. According to these figures, the measured strains at the two lateral faces are close to each other. It can be inferred that the brain stem behavior is similar to isotropic material. Based on Fig. 11, the lateral to longitudinal strain ratio at both directions is approximately 0.5, which is the Poisson ratio of an incompressible material. Therefore, it can be concluded that the brain stem is an incompressible material. Further, the results of analyzing these samples indicated that isotropy does not depend on the loading rate. The samples were taken from all parts of the brain stem. In another approach, the stress–strain diagrams resulting from the compressive loading applied at two strain rates of 1/60 s and 1/6 s was compared (Fig. 12). It can be observed from the results of experimental samples at two different strain rates that brain stem behaves similar to an isotropic material at different loading rates. Note that both of the approaches concluded the same results about the brain stem isotropy and the effect of loading rate on it.

The DIC method was used to analyze the isotropy of corona radiata. DIC analysis of corona radiata samples revealed that this part of brain is also isotropic. The isotropy of all samples was investigated at two different loading rates. Figure 13a shows comparison of strains measured on lateral faces when loading direction was along the dominant fiber direction. Similarly, Fig. 13b demonstrates the results of applying pressure perpendicular to the axons and

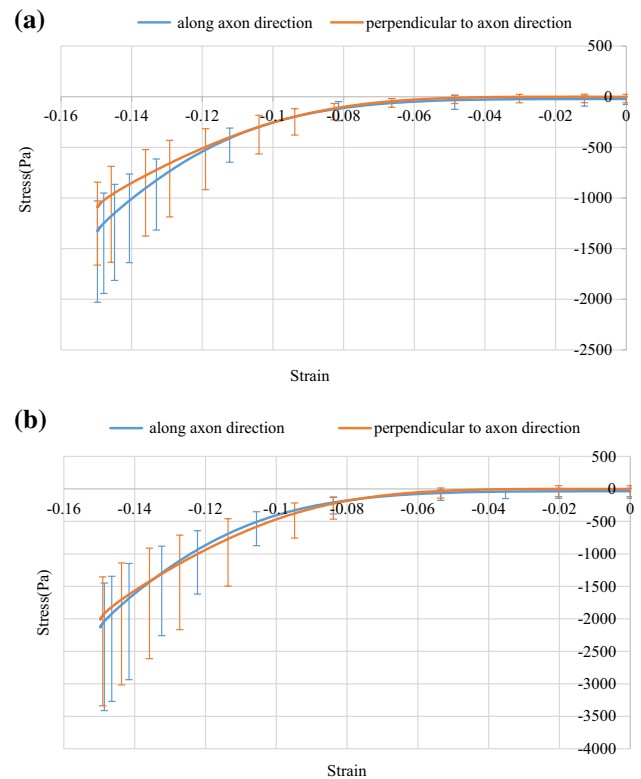


**Fig. 12** Average stress resulting from the pressure exerted on 20 samples of the brain stem; **a** at the rate of 1/60 s and **b** at the rate of 1/6 s

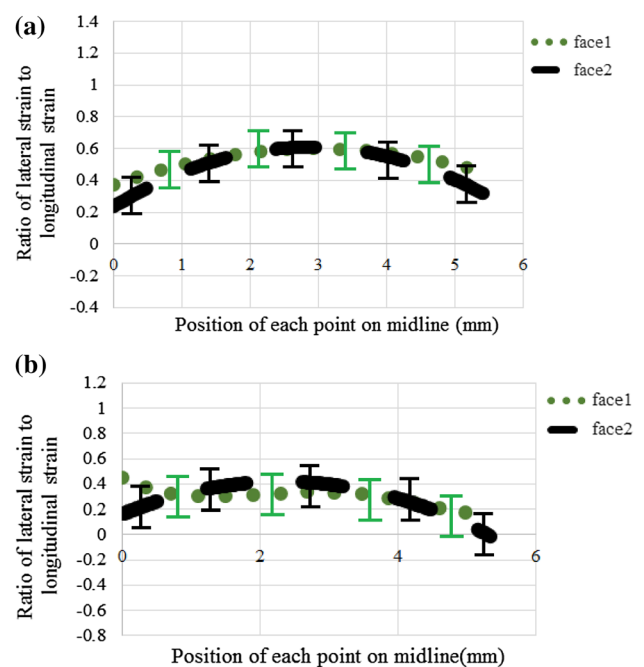


**Fig. 13** Comparison of the strain measured on face 1 and face 2 for 20 samples of the corona radiata through a midline; **a** applied load was parallel to the axons; **b** applied load was perpendicular to the axons

the measured lateral strains at the lateral faces. As can be observed in these figures, the measured strains are similar, suggesting that corona radiata shows no significant orientation dependency under compression load. Also, the lateral to longitudinal strain ratio was approximately 0.5, proving the incompressibility of corona radiata. Comparison of the obtained stress–strain curves from tests on corona radiata specimens with different orientations suggests that this part of brain is also isotropic, thereby validating the results of DIC approach (Fig. 14).

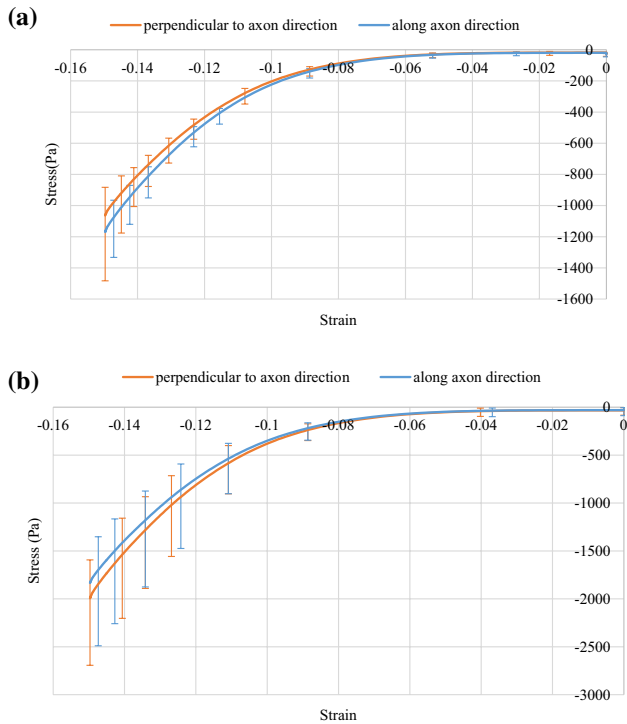


**Fig. 14** Average stress resulting from pressure exerted on 20 samples of the corona radiata; **a** at the rate of 1/60 s and **b** at the rate of 1/6 s

Table 2 shows measured lateral strain using the DIC method. The ratios of lateral strains to the longitudinal strains were measured across the middle lines of lateral faces for each specimen. Strains were measured up to 350 points of the midline. Each number represents the average of this ratio for one face of a specimen. Variation along each line is shown in Figs. 11 and 13. The amount of standard deviation is also included. At the end, the average values of data are reported for similar tests to investigate the anisotropic behavior of brain parts. The last line of this table shows isotropy and incompressibility of the brain tissue as discussed earlier.

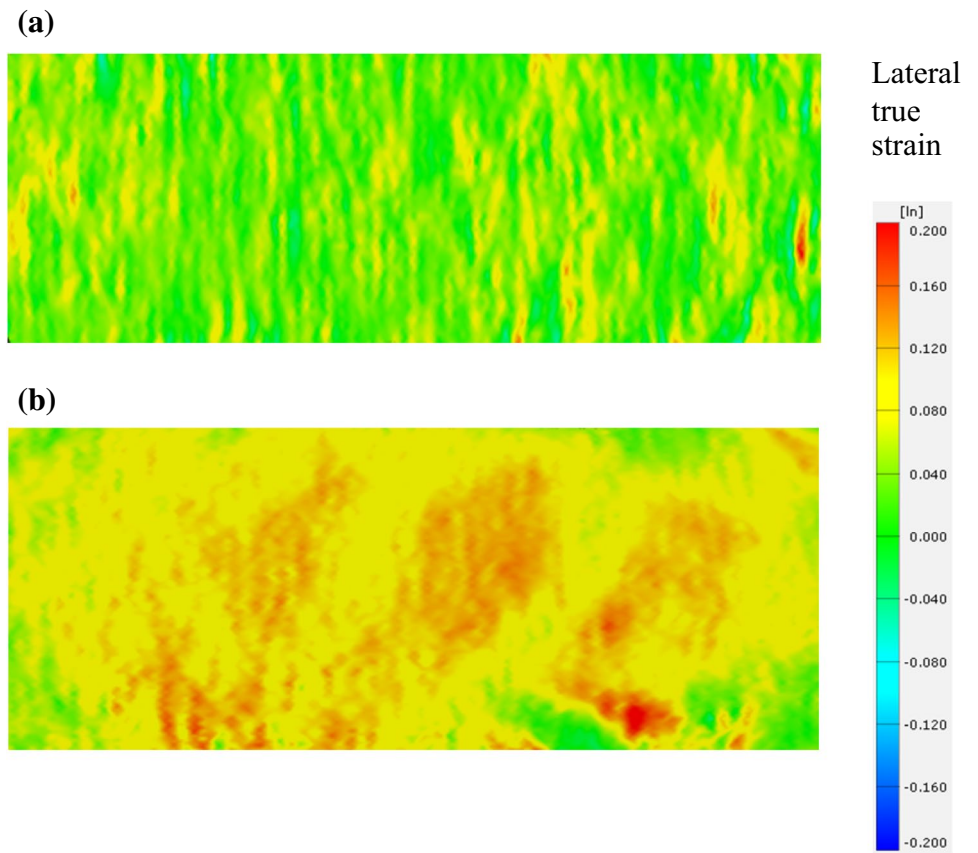
The laboratory samples of mixed white and gray matter showed no repeatable behavior. The results are dependent on how the white and gray matters are arranged in the samples. In this case, the samples were a mixture of two different materials with different mechanical properties, whose geometry strongly affected the overall behavior of the sample. Therefore, the results of different samples were not consistent and in some cases the tissue indicated isotropic behavior while in some others it presented anisotropic behavior. A typical anisotropic and isotropic behavior of mixed gray and white matter is illustrated in Figs. 15 and 16, respectively. The heterogeneous deformation distribution of different parts of the brain is very evident in all of the results of the DIC approach. However, in samples containing both white and gray matter (e.g., Fig. 15 and 16), a higher level of heterogeneity was observed. On the other hand, the results of stress–strain diagrams in two different directions for two specimens revealed that the orientation dependency varies from specimen to specimen (Fig. 17). These results suggest the agreement of the DIC method and stress–strain curves again.

Based on the current findings, the mechanical behavior of mixed white and gray matter alters across different specimens. This could be one reason for the contradictory results of previous experiments. Some studies, in which the

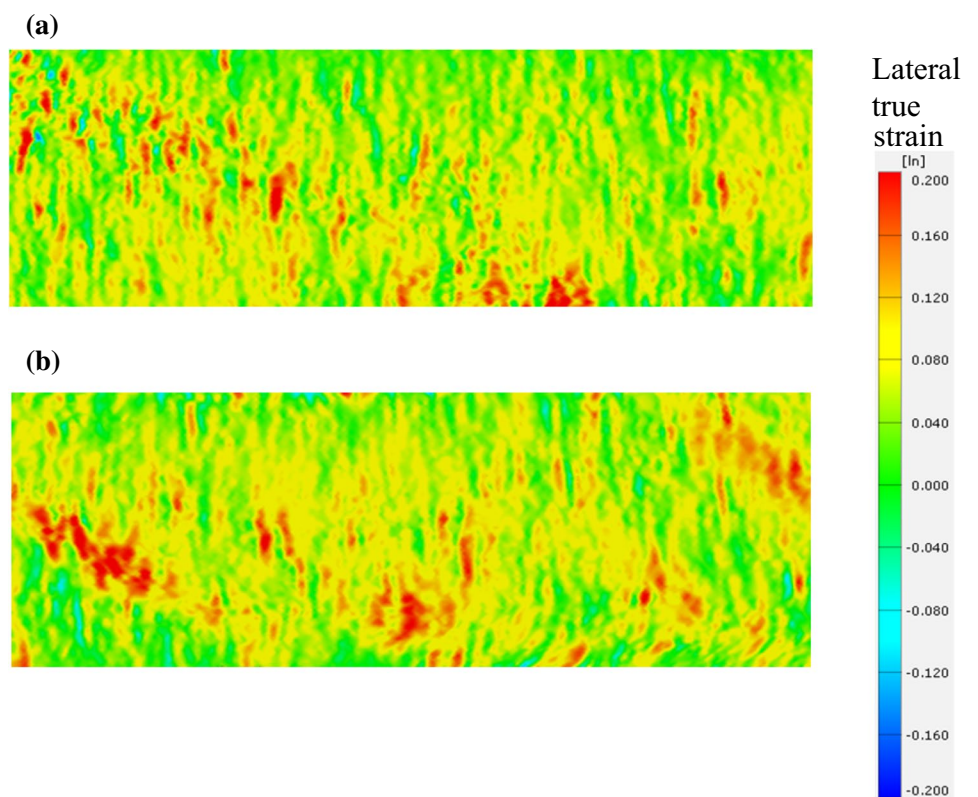
**Table 2** Measured lateral to longitudinal strain ratio across the middle lines of various samples using DIC method

Specimen number	Brain stem—along the fiber direction		Brain stem—perpendicular to the fiber direction		Corona radiata—perpendicular to the dominant fiber direction		Corona radiata—along the direction of dominant fiber	
	Face1	Face2	Face1	Face2	Face1	Face2	Face1	Face2
1	0.412 ± 0.0525	0.541 ± 0.0681	0.379 ± 0.0684	0.457 ± 0.0686	0.515 ± 0.0637	0.532 ± 0.0937	0.515 ± 0.0640	0.478 ± 0.0549
2	0.437 ± 0.0784	0.407 ± 0.0955	0.514 ± 0.0668	0.409 ± 0.0518	0.552 ± 0.0548	0.412 ± 0.0655	0.552 ± 0.0954	0.603 ± 0.0678
3	0.581 ± 0.0578	0.481 ± 0.0912	0.478 ± 0.0512	0.559 ± 0.0962	0.364 ± 0.0911	0.457 ± 0.0582	0.364 ± 0.0927	0.518 ± 0.0751
4	0.478 ± 0.0931	0.577 ± 0.0547	0.441 ± 0.0871	0.382 ± 0.0646	0.507 ± 0.0438	0.603 ± 0.0617	0.507 ± 0.0834	0.485 ± 0.0830
5	0.522 ± 0.0814	0.610 ± 0.0920	0.403 ± 0.0983	0.472 ± 0.0412	0.724 ± 0.0724	0.561 ± 0.0486	0.724 ± 0.0778	0.475 ± 0.0756
6	0.541 ± 0.0751	0.534 ± 0.0545	0.475 ± 0.0843	0.522 ± 0.0951	0.457 ± 0.0695	0.397 ± 0.0739	0.457 ± 0.0652	0.461 ± 0.0968
7	0.420 ± 0.0627	0.448 ± 0.0691	0.437 ± 0.0627	0.489 ± 0.0575	0.528 ± 0.0631	0.481 ± 0.0461	0.528 ± 0.0428	0.489 ± 0.0937
8	0.382 ± 0.0564	0.473 ± 0.0672	0.630 ± 0.0779	0.563 ± 0.0629	0.569 ± 0.0625	0.524 ± 0.0575	0.569 ± 0.0689	0.434 ± 0.0843
9	0.489 ± 0.0757	0.534 ± 0.0937	0.484 ± 0.0628	0.482 ± 0.0834	0.515 ± 0.0811	0.485 ± 0.0917	0.515 ± 0.0624	0.381 ± 0.0625
10	0.509 ± 0.0639	0.462 ± 0.0532	0.386 ± 0.0637	0.531 ± 0.0594	0.641 ± 0.0526	0.441 ± 0.0497	0.641 ± 0.0537	0.537 ± 0.0692
Mean ± SD	0.477 ± 0.0634	0.506 ± 0.0627	0.462 ± 0.0738	0.486 ± 0.0599	0.537 ± 0.0973	0.489 ± 0.0658	0.537 ± 0.0973	0.486 ± 0.0595

**Fig. 15** Strain contour of a mixed white and gray matter sample; **a** face1 and **b** face2 (it seems anisotropic behavior)



**Fig. 16** Strain contour of a mixed white and gray matter sample; **a** face1 and **b** face2 (It seems Isotropic behavior)



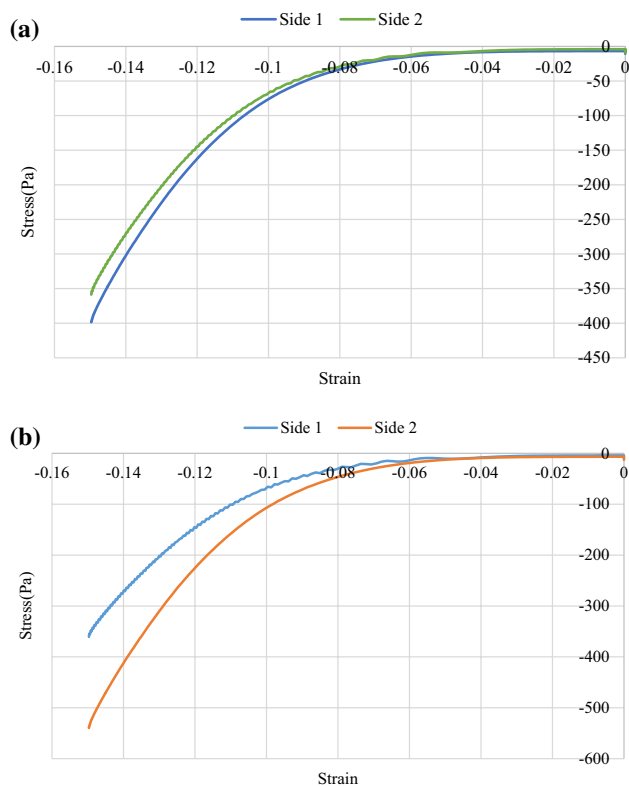


**Fig. 17** Stress resulting from the pressure exerted on 2 samples of the mixed white and gray matter at the rate of 1/60 s (the tests were conducted on both sides of each specimen) **a** first and **b** second mixed specimen

extracted white matter samples from the inner part of brain were too large, reported anisotropic behavior (Velardi et al. 2006; Feng et al. 2013). One reason for their claims is that they could not extract pure white matter and their extracted samples were a combination of white and gray matter.

It is worth mentioning that Figs. 11, 13, 15, and 16 show no uniformly distributed measured lateral strain on a face of a specimen. This heterogeneous distribution can be the result of:

- Using adhesion in the top and bottom surface of the specimen restricts the lateral movement of region near these surfaces but central region could deform without constraint. Therefore, a gradient of lateral strain exist in the specimens. To omit the effect of this variation, strains were measured at the middle lines of faces.
- Although efforts were done to extract appropriate samples from the brain tissue, the shapes of the specimens were not perfectly cubic, so strain variation was induced to the specimens.

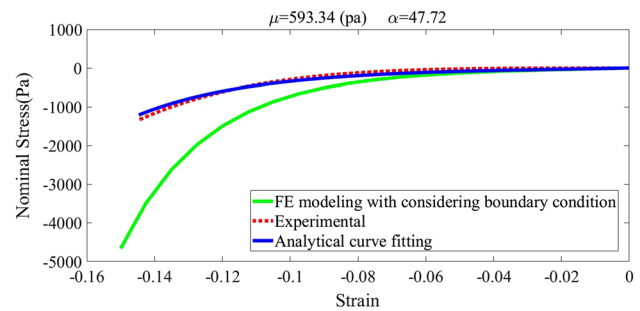


**Fig. 18** Comparison of experimental data, analytic curve fitting, and simulation results using the hyperelastic properties obtained from the analytical curve fitting

- Brain tissue parts, like other tissues of the body, have heterogeneous material behavior. In this research the specimens were taken as small as possible to reduce the effects of the material heterogeneity. This heterogeneity is more pronounced in mixed white and gray matter.

### 3.2 Evaluation of the direct fitting method for calculating material constants of the brain tissue

In this section, Ogden's hyperelastic model (Eq. 5) is calibrated with the test results of the compressive strain applied to the brain stem at the rate of 1/60 s. Then, the extracted hyperelastic constants including  $\mu$  and  $\alpha$  are used in a FE modeling, which considers the real boundary condition. Figure 18 indicates that using this type of calibration, there will be dramatic disparity between the experimental data and the simulation results. On the other hand, under real boundary conditions, cross-sectional area varies along the loading direction, where in the above calibration method a constant cross section was assumed all over the specimen. In other words, the stress and strain fields were taken as homogeneous. However, in the experimental samples, both the stress and strain were affected by boundary conditions and varied from point to point. Figure 19 depicts the distributions of the stress and strain resulting from the FE simulation using the material constants earned by analytical curve fitting. Figure 19 attests to the heterogeneity of the stress and strain fields under real boundary conditions. Further, the upper and lower faces of the model had stress concentration (highest stress) due to real conditions (adhesion). In the analytical fitting method, only the stress in the loading direction was considered and rest of the stress components were assumed to be zero. Figure 20 indicates the simulation results of the brain stem considering the real boundary conditions. It also represents the shear stresses on  $xy$ ,  $xz$ , and  $yz$  planes.

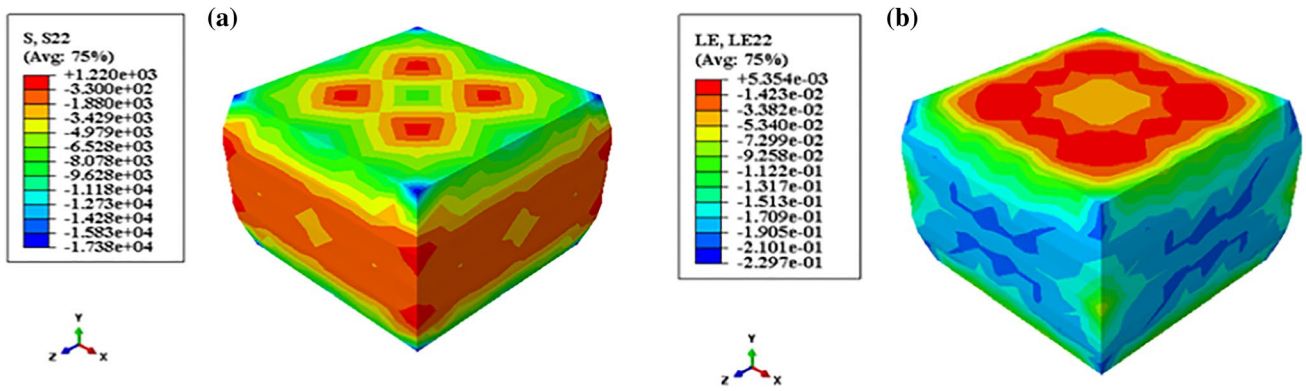


Fig. 19 Heterogeneity of strain and stress fields considering the experimental boundary conditions; **a** stress contour (Pa) and **b** strain contour

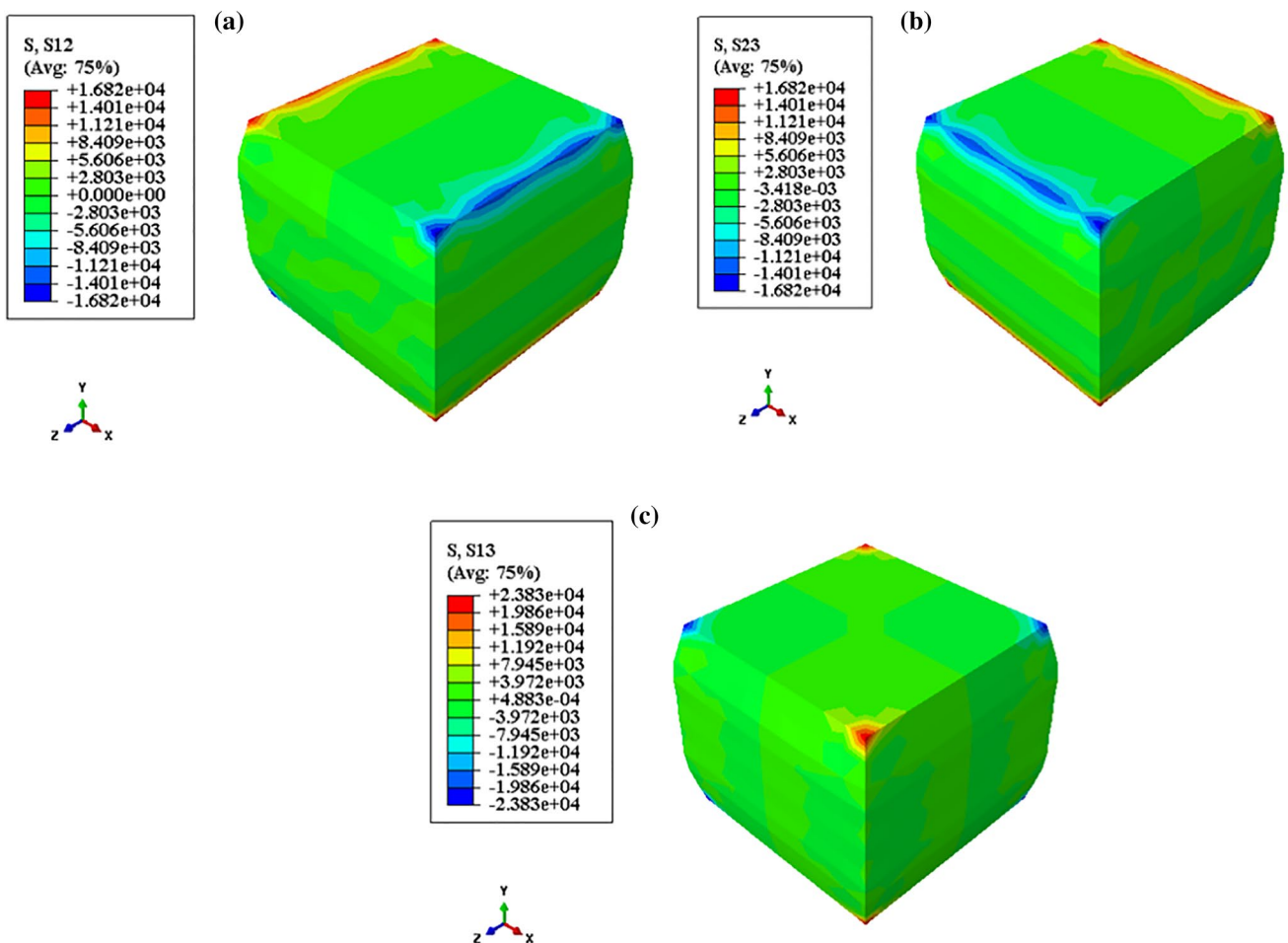


Fig. 20 Shear stress (in Pa) due to exerting uniaxial loading along planes **a**  $xy$ , **b**  $xz$ , and **c**  $yz$

Based on the results obtained in this section, it can be concluded that no accurate constants were obtained through the analytic fitting of the experimental data via Ogden’s model. The reason is that this approach assumes a uniform deformation for the entire sample and ignores

the induced stress components in relation to the stress in the loading direction. As a result, there will be significant differences between experimental and simulation results.

### 3.3 Extracting hyper-viscoelastic constants of the various parts of the brain tissue via inverse finite element modeling

As previously mentioned in Sect. 3.2, to extract the material constants of the brain tissue, the real boundary conditions should be taken into account in the FE modeling. Otherwise,

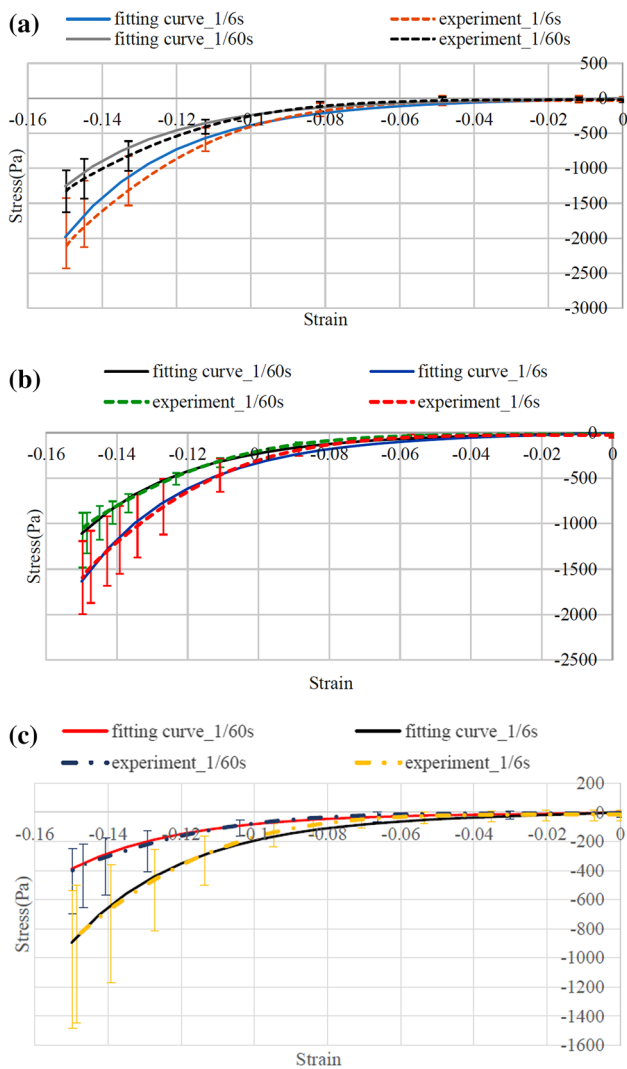


**Fig. 21** Fitting experimental data at the rates of 1/6 s and 1/60 s through the present approach in; **a** 10 brain stem samples, **b** 10 corona radiata samples, and **c** 10 mixed white and gray matters samples

the extracted properties would not be accurate. Once the real boundary conditions are taken into account in FE modeling, correct hyper-viscoelastic constants of the brain stem and other parts of the brain tissue can be obtained. To find the material constants of the brain tissue, the experimental data should have been fitted simultaneously at the rates of 1/6 s and 1/60 s. The target function defined was the sum of differences of experimental results at each strain rate with the corresponding FE simulation results. The stress–strain curves obtained from experimental and FE modeling at different loading rates are shown in Fig. 21 for the brain stem, corona radiata, as well as mixed white and gray matter samples. As can be observed, good fitted stress–strain curves can be obtained by reverse FE modeling for both loading rates simultaneously. Also, Table 3 reports the extracted constants of the brain stem, corona radiata, and the mixed of white and gray matter via the presented approach.

To investigate the variation of the extracted constants in various specimens, statistical analysis was also done on parameters of each tests. For this purpose, a set of material constants were extracted for each test by PSO algorithm, and finally, average and variation of these values were reported. Table 4 shows the resulted data in this method. The final mean data which are calculated by this way are close to the ones that are reported on Table 3. In this table the variations of these parameters in various specimens are more obvious.

The  $\mu$  has been reported in previous researches (Velardi et al. 2006; Prange and Margulies 2002; Miller and Chinzei 2002; Budday et al. 2017b; Voyiadjis and Samadi-Dooki 2018; Prange and Meaney 2000) in the range of 180 to 2960 Pa and in current work is between 300 and 500 Pa for various parts of brain. Since this constant represents the initial shear modulus of the material it should be similar for various researches. A wide range of  $\alpha$ , can be seen in the literature. This is due to the fact that: there is not a unique value for  $\alpha$  that can fit to the experimental data. Moreover, sensitivity of the result to the variation of  $\alpha$  is very low. Figure 22 shows the comparison of different stress–strain curves for various  $\alpha$ . As shown in this figure using to so different value of  $\alpha$  can results in the same stress–strain curves. Parameters related to the rate dependency of the brain tissue are also in the range of the previous literature (Prange and Margulies 2002; Rashid et al. 2012; Miller and Chinzei 2002; Budday et al. 2017b; Prange and Meaney 2000). It is noteworthy that due to the wide range of the extracted

**Table 3** Hyper-viscoelastic constants for various parts of brain

Tissue	$\mu$ (Pa)	$\alpha$	$g_1$	$\tau_1$ (s)	$g_2$	$\tau_2$ (s)	$R^2$ (1/6 s)	$R^2$ (1/60 s)
Brain stem	495.59	46.60	0.54	0.91	0.12	0.79	0.9876	0.9888
Corona radiata	439.84	44.53	0.47	0.59	0.01	0.45	0.9865	0.9867
Mixed of white and gray matter	302.57	42.56	0.89	0.96	0.15	0.35	0.9857	0.9825

**Table 4** Resulted constants extracted for each test by PSO algorithm

Test number	Parameter	Brain stem	Corona radiata	Mixed specimen	Test number	Parameter	Brain stem	Corona radiata	Mixed specimen
1	$\mu(\text{Pa})$	392.41	481.68	342.12	6	$\mu(\text{Pa})$	537.94	481.91	257.54
	$\alpha$	41.2	49.32	48.32		$\alpha$	48.12	46.53	44.18
	$g_1$	0.44	0.41	0.94		$g_1$	0.49	0.51	0.86
	$\tau_1(\text{s})$	0.78	0.63	0.97		$\tau_1(\text{s})$	0.88	0.63	0.95
	$g_2$	0.08	0.015	0.18		$g_2$	0.14	0.013	0.14
2	$\tau_2(\text{s})$	0.65	0.38	0.46	7	$\tau_2(\text{s})$	0.72	0.77	0.42
	$\mu(\text{Pa})$	433.87	309.28	337.75		$\mu(\text{Pa})$	337.74	397.33	329.57
	$\alpha$	41.85	37.65	41.44		$\alpha$	30.24	41.87	40.99
	$g_1$	0.48	0.36	0.92		$g_1$	0.47	0.36	0.87
	$\tau_1(\text{s})$	0.75	0.64	0.91		$\tau_1(\text{s})$	0.94	0.58	0.95
3	$g_2$	0.14	0.009	0.16	8	$g_2$	0.04	0.005	0.14
	$\tau_2(\text{s})$	0.74	0.37	0.38		$\tau_2(\text{s})$	0.72	0.43	0.33
	$\mu(\text{Pa})$	571.91	529.11	385.62		$\mu(\text{Pa})$	402.82	298.82	413.51
	$\alpha$	48.67	46.12	44.75		$\alpha$	36.47	36.94	43.82
	$g_1$	0.62	0.51	0.81		$g_1$	0.44	0.40	0.93
4	$\tau_1(\text{s})$	0.89	0.54	0.99	9	$\tau_1(\text{s})$	0.83	0.64	0.98
	$g_2$	0.14	0.015	0.12		$g_2$	0.13	0.02	0.19
	$\tau_2(\text{s})$	0.88	0.33	0.41		$\tau_2(\text{s})$	0.70	0.39	0.38
	$\mu(\text{Pa})$	211.94	382.62	263.42		$\mu(\text{Pa})$	449.71	457.92	284.34
	$\alpha$	25.12	32.34	38.94		$\alpha$	38.91	42.27	38.22
5	$g_1$	0.38	0.51	0.86	10	$g_1$	0.37	0.49	0.80
	$\tau_1(\text{s})$	0.61	0.52	0.88		$\tau_1(\text{s})$	0.57	0.56	0.95
	$g_2$	0.09	0.011	0.13		$g_2$	0.07	0.001	0.11
	$\tau_2(\text{s})$	0.73	0.41	0.33		$\tau_2(\text{s})$	0.62	0.42	0.37
	$\mu(\text{Pa})$	463.36	410.28	218.55		$\mu(\text{Pa})$	562.14	389.61	277.63
	$\alpha$	42.78	39.77	34.91		$\alpha$	58.66	35.71	44.15
	$g_1$	0.61	0.44	0.75		$g_1$	0.52	0.44	0.88
	$\tau_1(\text{s})$	0.87	0.62	0.97		$\tau_1(\text{s})$	0.94	0.57	0.92
	$g_2$	0.13	0.011	0.2		$g_2$	0.07	0.012	0.14
	$\tau_2(\text{s})$	0.76	0.59	0.38		$\tau_2(\text{s})$	0.87	0.43	0.32
		Parameter	Brain stem	Corona radiata	Mixed specimen				
Mean $\pm$ SD		$\mu(\text{Pa})$	436.38 $\pm$ 109.83	413.85 $\pm$ 74.88	311.005 $\pm$ 61.09				
		$\alpha$	41.02 $\pm$ 9.52	40.852 $\pm$ 5.378632	41.972 $\pm$ 3.87				
		$g_1$	0.48 $\pm$ 0.079	0.443 $\pm$ 0.06	0.86 $\pm$ 0.06				
		$\tau_1(\text{s})$	0.80 $\pm$ 0.12	0.59 $\pm$ 0.04	0.94 $\pm$ 0.03				
		$g_2$	0.10 $\pm$ 0.03	0.01 $\pm$ 0.005	0.15 $\pm$ 0.03				

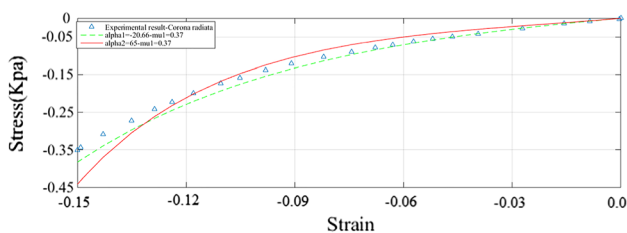


**Fig. 22** Stress–strain curves for various  $\alpha$

parameters that exist in the literature a meaningful difference cannot be observed between the current presented inverse finite element modeling and previous analytically fitted data.

### 4 Conclusions

The present research examined primary significant behaviors of the brain tissue which are still controversial. The anisotropic behavior of different parts of brain tissue was investigated by two approaches. DIC method, which has



been used in various biomechanical issues, was employed for the first time to investigate the isotropy of the brain tissue. To this aim, compression tests with two loading rates were performed on samples from various parts of brain tissue along two different directions with respect to the axonal fiber orientation. Then, the lateral strains were measured and compared to explore the isotropy of the different brain parts. Unlike studies which considered white matter as an anisotropic material, the current findings revealed that the brain stem and the corona radiata behave similar to isotropic materials. It was also observed that some of the mixed white and gray matter samples had anisotropic behavior, while other samples behaved like isotropic materials. Different geometrical shapes and arrangements of white and gray constituents can cause this discrepancy. All of DIC results revealed the heterogeneity and incompressibility of the different parts of the brain tissue.

The stress–strain diagrams of different parts of brain tissue showed that the brain stem and corona radiata are isotropic thereby validating the DIC data. Unlike white parts of brain, stress–strain diagrams of the mixed white and gray matter varied across different specimens. Further, the stress–strain diagrams of different parts of brain tissue indicated that all the constituent parts had a rate-dependent behavior, but the isotropy of the parts was not dependent on the loading rate.

In this study, it was also found that use of analytical curve fitting to extract mechanical constants of the brain tissue, which does not take into account the real boundary conditions, yields a remarkable error. To overcome this shortcoming, a precise calibration method was proposed for extracting mechanical constants. To this aim, a reverse FE model with the PSO algorithm was used to extract the hyper-viscoelastic constants of different parts of the brain tissue.

Note that although the DIC method is noninvasive in measuring displacement/strain fields of a sample, it has some shortcomings. For example, to generate a spackled surface, a complete surface preparation is required which prolongs the postmortem time.

Another shortcoming of the current research was failure to conduct tests on the corpus callosum. The corpus callosum part can be a perfect sample due to its specific microstructure, but the specimens extracted from the sheep brain tissue were very small.

Furthermore, the tests in this research were restricted to compression: firstly, because an appropriate testing machine was not available to conduct tests in different loading modes. Secondly, it has recently been shown that the critical state for brain tissue takes place in compression. Finally, the aim of this research was not presenting constitutive models; rather the most important goal was to

investigate the anisotropy and present an approach which extracts the material constants in a more accurate way.

## Compliance with ethical standards

**Conflict of interest** The authors declare that they have no conflict of interest.

## References

- Aimedieu P, Grebe R, Idy-Peretti I (2001) Study of brain white matter anisotropy. In: Engineering in medicine and biology society. Proceedings of the 23rd annual international conference of the IEEE, IEEE, vol 2, pp 1009–1011
- Anderson RW, Brown CJ, Blumbergs PC, McLean AJ, Jones NR (2003) Impact mechanics and axonal injury in a sheep model. *J Neurotrauma* 20(10):961–974
- Annaidh AN, Bruyère K, Destrade M, Gilchrist MD, Otténio M (2012) Characterization of the anisotropic mechanical properties of excised human skin. *J Mech Behav Biomed Mater* 5(1):139–148
- Arbogast KB, Margulies SS (1999) A fiber-reinforced composite model of the viscoelastic behavior of the brainstem in shear. *J Biomech* 32(8):865–870
- Bilston LE, Liu Z, Phan-Thien N (2001) Large strain behavior of brain tissue in shear: some experimental data and differential constitutive model. *Biorheology* 38(4):335–345
- Brunon A, Bruyere-Garnier K, Coret M (2010) Mechanical characterization of liver capsule through uniaxial quasi-static tensile tests until failure. *J Biomech* 43(11):2221–2227
- Budday S et al (2015) Mechanical properties of gray and white matter brain tissue by indentation. *J Mech Behav Biomed Mater* 46:318–330
- Budday S et al (2017a) Mechanical characterization of human brain tissue. *Acta Biomater* 48:319–340
- Budday S, Sommer G, Holzapfel G, Steinmann P, Kuhl E (2017b) Viscoelastic parameter identification of human brain tissue. *J Mech Behav Biomed Mater* 74:463–476
- Chatelin S et al (2011) Computation of axonal elongation in head trauma finite element simulation. *J Mech Behav Biomed Mater* 4(8):1905–1919
- Chatelin S, Vappou J, Roth S, Raul J-S, Willinger R (2012) Towards child versus adult brain mechanical properties. *J Mech Behav Biomed Mater* 6:166–173
- Christ AF et al (2010) Mechanical difference between white and gray matter in the rat cerebellum measured by scanning force microscopy. *J Biomech* 43(15):2986–2992
- Cloots R, Van Dommelen J, Nyberg T, Kleiven S, Geers M (2011) Micromechanics of diffuse axonal injury: influence of axonal orientation and anisotropy. *Biomech Model Mechanobiol* 10(3):413–422
- Cloots R, Van Dommelen J, Geers M (2012) A tissue-level anisotropic criterion for brain injury based on microstructural axonal deformation. *J Mech Behav Biomed Mater* 5(1):41–52
- Cloots RJ, Van Dommelen J, Kleiven S, Geers M (2013) Multi-scale mechanics of traumatic brain injury: predicting axonal strains from head loads. *Biomech Model Mechanobiol* 12(1):137–150
- Darvish K, Crandall J (2001) Nonlinear viscoelastic effects in oscillatory shear deformation of brain tissue. *Med Eng Phys* 23(9):633–645
- Donnelly B, Medige J (1997) Shear properties of human brain tissue. *J Biomech Eng* 119(4):423–432

- Elkin BS, Ilankovan A, Morrison B (2010) Age-dependent regional mechanical properties of the rat hippocampus and cortex. *J Biomech Eng* 132(1):011010
- Estes MS, McElhaney JH (1970) Response of brain tissue to compressive loading. *Mech Eng* 92:58–61
- Fallenstein G, Hulce VD, Melvin JW (1969) Dynamic mechanical properties of human brain tissue. *J Biomech* 2(3):217–226
- Feng Y, Okamoto RJ, Namani R, Genin GM, Bayly PV (2013) Measurements of mechanical anisotropy in brain tissue and implications for transversely isotropic material models of white matter. *J Mech Behav Biomed Mater* 23(117):132
- Feng Y, Lee C-H, Sun L, Ji S, Zhao X (2017) Characterizing white matter tissue in large strain via asymmetric indentation and inverse finite element modeling. *J Mech Behav Biomed Mater* 65:490–501
- Finan JD, Elkin BS, Pearson EM, Kalbian IL, Morrison B (2012) Viscoelastic properties of the rat brain in the sagittal plane: effects of anatomical structure and age. *Ann Biomed Eng* 40(1):70–78
- Franceschini G, Bigoni D, Regitnig P, Holzapfel GA (2006) Brain tissue deforms similarly to filled elastomers and follows consolidation theory. *J Mech Phys Solids* 54(12):2592–2620
- Galford JE, McElhaney JH (1970) A viscoelastic study of scalp, brain, and dura. *J Biomech* 3(2):211–221
- Garcia-Gonzalez D, Jérusalem A, Garzon-Hernandez S, Zaera R, Arias A (2018) A continuum mechanics constitutive framework for transverse isotropic soft tissues. *J Mech Phys Solids* 112:209–224
- Giordano C, Kleiven S (2014) Evaluation of axonal strain as a predictor for mild traumatic brain injuries using finite element modeling. SAE technical paper
- Giordano C, Cloots R, Van Dommelen J, Kleiven S (2014) The influence of anisotropy on brain injury prediction. *J Biomech* 47(5):1052–1059
- Goriely A et al (2015) Mechanics of the brain: perspectives, challenges, and opportunities. *Biomech Model Mechanobiol* 14(5):931–965
- Hrapko M, Van Dommelen J, Peters G, Wismans J (2008a) Characterisation of the mechanical behavior of brain tissue in compression and shear. *Biorheology* 45(6):663–676
- Hrapko M, Van Dommelen J, Peters G, Wismans J (2008b) The influence of test conditions on characterization of the mechanical properties of brain tissue. *J Biomech Eng* 130(3):031003
- Javid S, Rezaei A, Karami G (2014) A micromechanical procedure for viscoelastic characterization of the axons and ECM of the brainstem. *J Mech Behav Biomed Mater* 30:290–299
- Jin X, Zhu F, Mao H, Shen M, Yang KH (2013) A comprehensive experimental study on material properties of human brain tissue. *J Biomech* 46(16):2795–2801
- Karimi A, Navidbakhsh M (2014) An experimental study on the mechanical properties of rat brain tissue using different stress–strain definitions. *J Mater Sci Mater Med* 25(7):1623–1630
- Karimi A, Navidbakhsh M, Yousefi H, Haghi AM, Sadati SA (2014) RETRACTED: experimental and numerical study on the mechanical behavior of rat brain tissue. *Perfusion* 29(4):307–314
- Lauret C, Hrapko M, Van Dommelen J, Peters G, Wismans J (2009) Optical characterization of acceleration-induced strain fields in inhomogeneous brain slices. *Med Eng Phys* 31(3):392–399
- Lee W, Lee SD, Park MY, Foley L, Purcell-Estabrook E, Kim H et al (2015) Functional and diffusion tensor magnetic resonance imaging of the sheep brain. *BMC Vet Res* 11(1):262
- Lewis SB et al (1996) A head impact model of early axonal injury in the sheep. *J Neurotrauma* 13(9):505–514
- Libertiaux V, Pascon F, Cescotto S (2011) Experimental verification of brain tissue incompressibility using digital image correlation. *J Mech Behav Biomed Mater* 4(7):1177–1185
- Mihai LA, Chin L, Janmey PA, Goriely A (2015) A comparison of hyperelastic constitutive models applicable to brain and fat tissues. *J R Soc Interface* 12(110):20150486
- Mihai LA, Budday S, Holzapfel GA, Kuhl E, Goriely A (2017) A family of hyperelastic models for human brain tissue. *J Mech Phys Solids* 106(60):79
- Miller K (1999) Constitutive model of brain tissue suitable for finite element analysis of surgical procedures. *J Biomech* 32(5):531–537
- Miller K, Chinzei K (1997) Constitutive modelling of brain tissue: experiment and theory. *J Biomech* 30(11):1115–1121
- Miller K, Chinzei K (2002) Mechanical properties of brain tissue in tension. *J Biomech* 35(4):483–490
- Miller K, Chinzei K, Orsengo G, Bednarsz P (2000) Mechanical properties of brain tissue in vivo: experiment and computer simulation. *J Biomech* 33(11):1369–1376
- Ning X, Zhu Q, Lanir Y, Margulies SS (2006) A transversely isotropic viscoelastic constitutive equation for brainstem undergoing finite deformation. *J Biomech Eng* 128(6):925–933
- Ogden RW (1972) Large deformation isotropic elasticity—on the correlation of theory and experiment for incompressible rubberlike solids. *Proc R Soc Lond A* 326(1567):565–584
- Pamiljans V, Krishnaswamy P, Dumville G, Meister A (1962) Studies on the mechanism of glutamine synthesis; isolation and properties of the enzyme from sheep brain. *Biochemistry* 1(1):153–158
- Pan B, Qian K, Xie H, Asundi A (2009) Two-dimensional digital image correlation for in-plane displacement and strain measurement: a review. *Meas Sci Technol* 20(6):062001
- Prange M, Meaney DF (2000) Defining brain mechanical properties: effects of region, direction, and species (no 2000-01-SC15). SAE technical paper extraction of brain stem sample
- Prange MT, Margulies SS (2002) Regional, directional, and age-dependent properties of the brain undergoing large deformation. *J Biomech Eng* 124(2):244–252
- Rashid B, Destrade M, Gilchrist MD (2012) Mechanical characterization of brain tissue in compression at dynamic strain rates. *J Mech Behav Biomed Mater* 10:23–38
- Rashid B, Destrade M, Gilchrist MD (2013) Mechanical characterization of brain tissue in simple shear at dynamic strain rates. *J Mech Behav Biomed Mater* 28:71–85
- Rashid B, Destrade M, Gilchrist MD (2014) Mechanical characterization of brain tissue in tension at dynamic strain rates. *J Mech Behav Biomed Mater* 33:43–54
- Shuck L, Advani S (1972) Rheological response of human brain tissue in shear. *J Basic Eng* 94(4):905–911
- Thibault KL, Margulies SS (1998) Age-dependent material properties of the porcine cerebrum: effect on pediatric inertial head injury criteria. *J Biomech* 31(12):1119–1126
- Tse KM, Tan LB, Lee SJ, Lim SP, Lee HP (2014) Development and validation of two subject-specific finite element models of human head against three cadaveric experiments. *Int J Numer Methods Biomed Eng* 30(3):397–415
- Van Dommelen J, Van der Sande T, Hrapko M, Peters G (2010) Mechanical properties of brain tissue by indentation: interregional variation. *J Mech Behav Biomed Mater* 3(2):158–166
- Velardi F, Fraternali F, Angelillo M (2006) Anisotropic constitutive equations and experimental tensile behavior of brain tissue. *Biomech Model Mechanobiol* 5(1):53–61
- Voyiadjis GZ, Samadi-Dooki A (2018) Hyperelastic modeling of the human brain tissue: effects of no-slip boundary condition and compressibility on the uniaxial deformation. *J Mech Behav Biomed Mater* 83:63–78

Wright RM, Post A, Hoshizaki B, Ramesh KT (2013) A multiscale computational approach to estimating axonal damage under inertial loading of the head. *J Neurotrauma* 30(2):102–118

Wu LC et al (2016) In vivo evaluation of wearable head impact sensors. *Ann Biomed Eng* 44(4):1234–1245

Zhang DS, Arola DD (2004) Applications of digital image correlation to biological tissues. *J Biomed Opt* 9(4):691–700

**Publisher's Note** Springer Nature remains neutral with regard to jurisdictional claims in published maps and institutional affiliations.